392 J. Med. Chem. 2010, 53, 392–401
DOI: 10.1021/jm901421c

Journal of Medicinal Chemistry Article

The Permeation of Amphoteric Drugs through Artificial Membranes − An in Combo Absorption Model Based on Paracellular and Transmembrane Permeability†

Kin Y. Tam,*,‡ Alex Avdeef,*,§ Oksana Tsinman,§ and Na Sun§

‡AstraZeneca, Mereside, Alderley Park, Macclesfield, Cheshire SK10 4TG, U.K. and §pION INC, 5 Constitution Way, Woburn, Massachusetts 01801. †Contribution number 26 in the PAMPA − A Drug Absorption in Vitro Model series from pION. Reference 59 is part 25 in the series.

Received September 24, 2009

The permeability characteristics of 33 amphoteric drugs (about 64% zwitterions at physiological pH) were studied using the parallel artificial membrane permeability assay (PAMPA) at pH 6.5. The PAMPA data were modified to include the paracellular permeability component found in cellular monolayers based on a newly generalized version of a popular model devised for Caco-2 cells. These "in combo" PAMPA data were used to predict the human absolute bioavailability of the ampholytes. The analysis produced a good fit, with only five outliers whose transport properties, could be rationalized by (a) nonpassive permeability processes, (b) metabolic instability, and (c) the possible sensitivity to microclimate pH effects in the case of acidic ampholytes. With the exception of two compounds, all of the ampholytes with bioavailability < 50% were predominantly transported by the paracellular route, surprisingly with several of the compounds having molecular weights exceeding 350 Da.

Introduction

Amphoteric compounds are used as drugs in various therapeutic areas. These compounds consist of at least one acidic group and at least one basic group, where the pK_a (acid dissociation constants) values are of comparable magntitude.[1] Taking a diprotic amphoteric compound as an example, the molecule could exist in four different pH-dependent protonation forms, namely cation (H_2X^+),[a] zwitterions ($HX^{\pm}$), neutral species (HX^0), and anion (X^-), which are shown in Figure 1. In contrast to other ionizable drugs with only acidic or basic group(s), an amphoteric drug exhibits unique physicochemical and pharmacokinetic properties. For example, the volume of distribution is usually lower than that of a basic drug, which suggests that the amphoteric drug tends to stay in the plasma. Because the molecule is predominately charged across the physiological pH region, the lipophilicity tends to be low to moderate. These properties would be better suited for the drug targets located in the plasma because the distribution into tissues/organs is not favorable for this kind of compound. Amphoteric drugs have been shown to be beneficial in some clinical applications.[2] Typical examples are antibacterials, antiallergics, and diuretics.

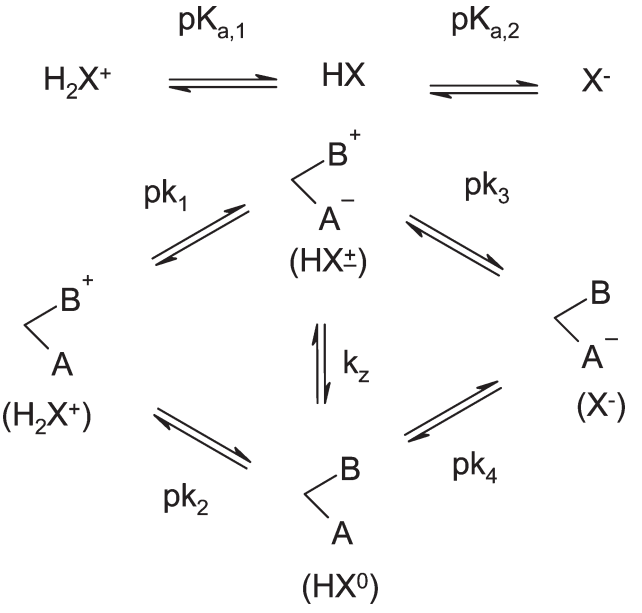

Figure 1. Ionization scheme of a diprotic amphoteric molecule.

According to the pH-partition hypothesis, absorption is favored for the neutral form of the drug molecule.[3] For amphoteric compounds where the zwitterionic form is the

*To whom correspondence should be addressed. For K.Y.T.: phone, +44 (0)1625 230338; fax, +44 (0)1625 510097; e-mail, kin.tam@astrazeneca.com. For A.A.: phone, +1 781 935 8939; fax, +1 781 935 8938; e-mail, aavdeef@pion-inc.com.

[a] Abbreviations: H_2X^+, cation; $HX^{\pm}$, zwitterions; HX^0, neutral species; X^-, anion; PAMPA, parallel artificial membrane permeability assay; HDM, hexadecane; R, membrane junction pore radius; $\Delta\varphi$, voltage drop across a cellular membrane; ε/δ, porosity-path length ratio; D_{aq}, aqueous diffusivity; $F(r/R)$, Renkin molecular sieving function; $E(\Delta\varphi)$, function due to potential drop across the cell junction; r, molecular radius; $f_{(\pm/0)}$, concentration fraction of amphoteric molecule in the uncharged form (zwitterionic/neutral); $f_{(+)}$, concentration fraction of cation; $f_{(-)}$, concentration fraction of anion; P_e, effective PAMPA permeability coefficient; pH_{IEP}, isoelectric point pH; $P_{\pm/0}$, intrinsic permeability of the zwitterion/ampholyte (net zero charge) species; P_{mem}, membrane permeability; P_{ABL}, aqueous boundary layer permeability coefficient; h_{ABL}, aqueous boundary layer thickness; P_{para}, paracellular permeability; P_{trans}, transcellular permeability; P_e^{INT}, effective passive permeability at the intestinal cell membrane barrier; A (or B), fitting constant for the plug-flow absorption model; %F, human absolute bioavailability; %Para, relative fraction of transport effected by the paracellular route; %Trans, relative fraction of transport effected by the transcellular route; P_{app}, apparent cellular (Caco-2) permeability, log P_{OCT}, octanol−water partition coefficient; log D_{OCT}, octanol−water distribution coefficient.

 Published on Web 11/30/2009

predominant species, it would be expected that the absorption along the gastrointestinal tract would be low. Jamieson et al.[4] have pointed out that the formation of zwitterions is one of the successful approaches to attenuate the human ether-a-go-go related gene (hERG) liability, but this could lead to poor membrane permeability and consequently reduce the oral bioavailability of the compounds. Transporters expressed in the lumen, such as P-gp (P-glycoprotein) and OAT (organic anion transporter), could have a role in the efflux/active uptake of the compound.[5,6] Oral bioavailability is influenced by a number of factors such as the permeability of the compound across the lumen, the expression level and the saturability of the transporters, the therapeutic dose, and the in vivo metabolic behavior of the compound. Nevertheless, it is generally believed that the development of bioavailable amphoteric compounds to a drug is likely to be more challenging than compounds of other charge types, which may be partly due to the lack of understanding of the factors governing the membrane permeability of amphoteric compounds. Given that ampholytes, particularly zwitterions, are expected to be poorly absorbed by transmembrane passive diffusion processes, the availability of junctional pores in the intestinal epithelium posed the possibility of absorption via the paracellular route, where small hydrophilic solvated zwitterions could diffuse through water-filled channels between the cells. Such channels are known to be capacity-limited, size-restricted, and cation-selective, thus attenuating free diffusion in the water phase.

Recently, the parallel artificial membrane permeability assay (PAMPA) has emerged as an alternative physicochemical technique in the pharmaceutical industry for the determination passive permeability of research compounds.[7−13] There are several variants of PAMPA in current use,[11,12] with two popular models being the Double-Sink[8] and the hexadecane[9] (HDM) PAMPA. It was shown that Double-Sink PAMPA permeability values were consistently greater in magnitude than those of HDM PAMPA, with molecules like metoprolol showing differences as high as a 1000 between Double-Sink and HDM values.[11] Abraham descriptors were used to rationalize these observations. Briefly, water-solubilized polar molecules, especially zwitterions, form very strong H-bonds with the solvent. Such molecules need to break these bonds in order to enter the pure alkane phase, which is devoid of H-bond solvation. Hence, more energy may be needed for a polar molecule to penetrate a pure alkane barrier compared to a barrier possessing some H-bond interactions. The 20% phospholipid content of the Double-Sink lipid may ease the permeation process by offering a compensating source of H-bonding within the membrane phase. Consequently, the HDM model is not expected to be suitable for measuring the permeability of zwitterionic compounds. A quantitative comparison between two models[11] suggests that the predicted HDM permeability coefficients for some common zwitterions (e.g., chlortetracycline, demeclocycline, doxycycline, famotidine, lisinopril, minocycline, terbutaline, and tetracycline) would be less than 10^{-11} cm/s, well below the threshold of common detection methods.

A simple passive diffusion permeability model would not be expected to accurately predict the intestinal absorption of the smaller hydrophilic zwitterions because the paracellular route of absorption would not be adequately addressed. To remedy this, Sugano and co-workers[15−17] proposed adding to measured PAMPA values a calculated contribution expected for the paracellular route in their study of the absorption properties of a general class of drugs. It was thought here that their strategy would be particularly relevant for modeling zwitterion intestinal absorption. In the present study, we adopted a similar "combination" in silico−in vitro approach and selected the computational paracellular model developed by a thorough study of the cultured cell line, Caco-2, by Adson et al.[18]

In this work, we measured the passive permeability of 33 amphoteric compounds (Figure 2) using the Double-Sink PAMPA technique. These compounds can be broadly classified into several distinct series, namely, antibacterial (β-lactams, fluoroquinolones, tetracyclines), antihistamine (cetirizine, fexofenadine), anti-inflammatory (piroxicam, meloxicam), antiviral (acyclovir, ganciclovir), and diuretics (famotidine, torsemide), as well as a few key compounds, such as terbutaline (bronchodilator), melphalan (antineoplastic), cerivastain (antihyperlipoproteinemic), which represent some of the commonly used amphoteric drugs to-date. We deliberately selected compounds where the first pass effects are low to moderate and with published human absolute bioavailability uniformly distributed between high and low values. We developed models in this study to rationalize the permeability of these compounds. It is envisaged that this study will shed some light toward the predictions of the absorption of amphoteric compounds by PAMPA models.

Theoretical Section

In this study, the PAMPA model was extended to include a calculated paracellular component to better represent the effect of the epithelial cell junctions found in the human intestine. A similar approach was described by Sugano and co-workers[15−17] and recently applied by Reynolds et al.[19] Whereas the former investigators determined junction pore radius (R) and voltage drop ($\Delta\varphi$) by curve fitting PAMPA values directly to intestinal absorption data, the strategy used here is tied to a paracellular model developed using published Caco-2 data.

Paracellular Permeability Analysis (Pore Radius, Porosity−Path Length, and Potential Gradient). Adson and co-workers[18,20] proposed the general expression for paracellular permeability,

$$P_{\text{para}} = \left(\frac{\varepsilon}{\delta}\right)\cdot D_{\text{aq}}\cdot F\left(\frac{r}{R}\right)\left[f_{(\pm/0)} + f_{(+)}\cdot\frac{\kappa|\Delta\varphi|}{1-e^{-\kappa|\Delta\varphi|}} + f_{(-)}\cdot\frac{\kappa|\Delta\varphi|}{e^{+\kappa|\Delta\varphi|}-1}\right] \quad (1)$$

The (ε/δ) term represents the porosity−path length ratio, where the porosity, ε, is the relative surface area of the junction opening divided by the total epithelial surface area, and the path length, δ, represents the thickness of the restricted-junction domain times the tortuosity of the paracellular route. D_{aq} ($\text{cm}^2\ \text{s}^{-1}$) is the aqueous diffusivity, which was estimated at 25 °C using the empirical function[8,21,22] of the molecular weight (MW): $D_{\text{aq}} = 10^{\{-4.131-0.453\log\text{MW}\}}$. $F(r/R)$ is the Renkin molecular sieving function, which is a polynomial function (with values ranging from 0 to 1) of the ratio of the hydrodynamic radius of the solute, r, to the apparent paracellular pore radius, R, taken up to the seventh power.[18,20] If the molecular radius exceeds that of the pore, the paracellular route is completely blocked according to eq 1 because $F(r/R) = 0$. The smaller the molecule is in relation to the pore radius, the closer is $F(r/R)$ to 1. With D_{aq} at hand (above), the molecular radius, r, can be estimated from the

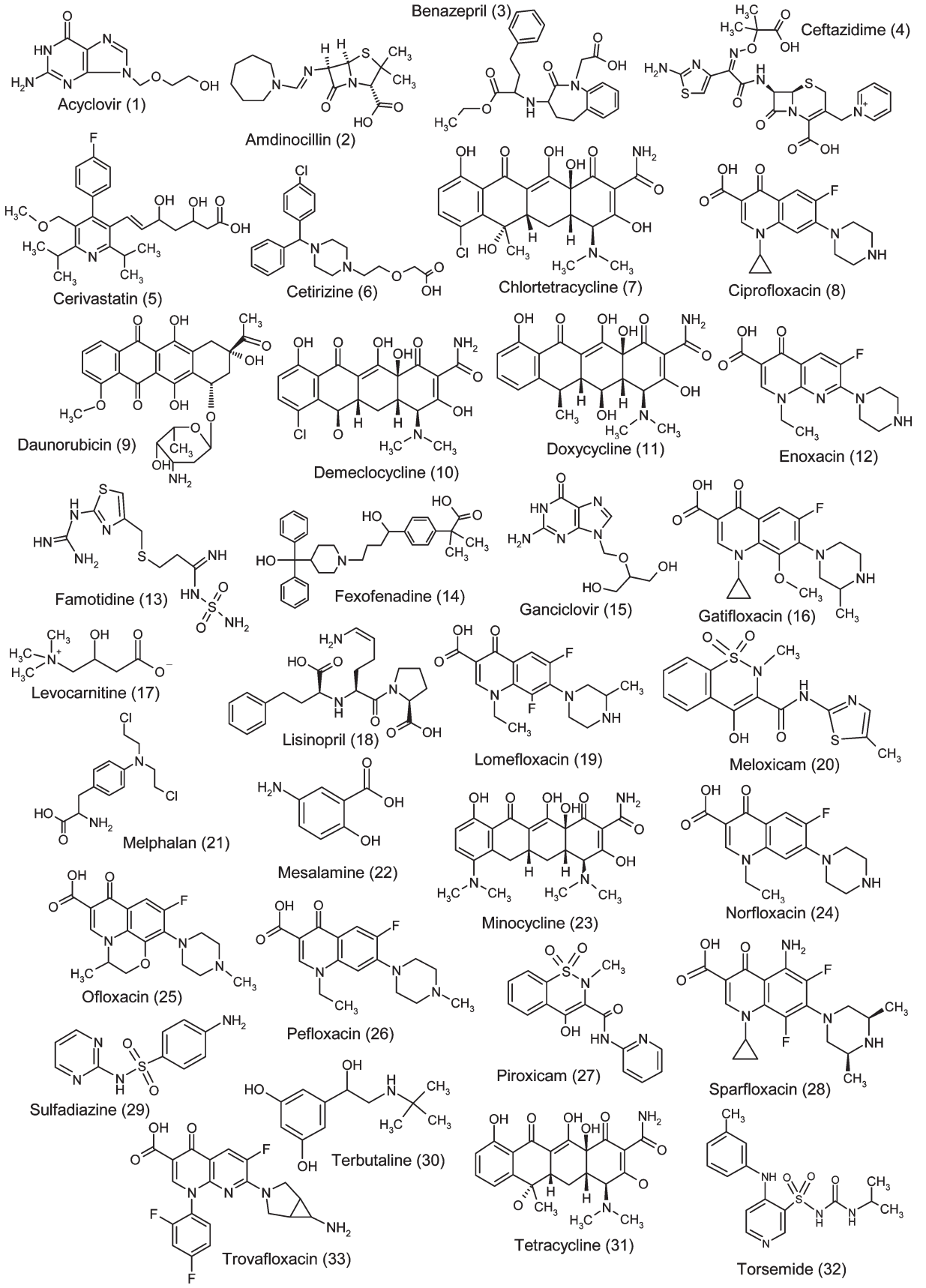

Figure 2. Structure of the 33 amphoteric drugs.

Sutherland−Stokes−Einstein spherical-molecule equation as $r(\text{Å}) = 10^{+8}\ k_B T/(g\pi\eta D_{aq})$, where η is the kinematic viscosity (0.00893 poise at 25 °C), k_B is the Boltzmann constant, T is the absolute temperature, and g is a constant whose value is between 4 (small molecule limit) and 6 (large molecule limit).[22] The square-bracket term in eq 1, which

may be called $E(\Delta\varphi)$ hereon, is a function of the electrical potential drop, $\Delta\varphi$ (mV), across the junction created by negatively charge residues (carboxylate and phosphate) lining the junctional pores, where $f_{(\pm/0)}$, $f_{(+)}$, and $f_{(-)}$ are the concentration fractions of the amphoteric molecule in the uncharged (zwitterionic/neutral), cationic, and anionic forms, respectively (where $f_{(\pm/o)} + f_{(+)} + f_{(-)} = 1$); $\kappa = F/(k_B T N_A)$, where N_A is the Avogadro number, and F is the Faraday constant. The term in the brackets, $E(\Delta\varphi)$, is 1 for neutral molecules, about 1.4 for cations, and 0.7 for anions.

Adson and co-workers[18,20] proposed the estimates: $(\varepsilon/\delta) = 1.22\ \text{cm}^{-1}$, $R = 12$ Å, and $\Delta\varphi = -17.7$ mV, based on the Caco-2 permeability of nine paracellular markers (both neutral and charged). Our reanalysis produced slightly different set of constants.

As part of a broader study,[22] we compared the leakiness and size exclusion of the paracellular channels in 14 cultured epithelial cell monolayer studies (mostly Caco-2, but also MDCK, and 2/4/A1), with data taken from eight laboratories (including that of Adson et al.[19]). The mathematical calculations are described in full detail in the expanded study.[22] Briefly stated, we re-evaluated the cellular permeability data using a newly developed paracellular model refinement method included in the *p*CEL-X v2.0 program (*p*ION). The (ε/δ), R, and $\Delta\varphi$ parameters (along with those defining the aqueous boundary layer contributions and those related to transcellular permeability) were determined simultaneously by a generalized nonlinear weighted regression analysis. The Adson Caco-2 cells were relatively leaky among the Caco-2 sets in the interlaboratory study and thought here to be a suitable model for application to human intestinal absorption prediction.

Zwitterion/Ampholyte Permeability. The effective PAMPA permeability coefficients, P_e, at the isoelectric point pH (pH_{IEP}) and the ionization constants (pK_a) of the zwitterions/ampholytes were used to determine the intrinsic permeability, $P_{\pm/0}$, by regression analysis, using the permeability coefficients refinement function in the *p*CEL-X program. P_e is related to the artificial membrane and the aqueous boundary layer (ABL) permeability coefficients, P_{mem} and P_{ABL}, respectively, as

$$\frac{1}{P_e} = \frac{1}{P_{ABL}} + \frac{1}{P_{mem}} \tag{2}$$

where P_{ABL} is defined as the ratio D_{aq}/h_{ABL}. The ABL thickness, h_{ABL}, was calculated by the program (about 40 and 1500 μm for stirred and unstirred PAMPA data, respectively, depending on the molecular weight of the drug). For ionizable molecules, the membrane permeability, P_{mem}, depends on pH of the bulk aqueous solution. The maximum possible P_{mem} is designated $P_{\pm/0}$, the apparent intrinsic permeability of the zwitterion/ampholyte (net zero charge) species. The relationship between P_{mem} and $P_{\pm/0}$ may be stated as

$$\frac{1}{P_{mem}} = \frac{10^{-pH+pK_{a,1}} + 10^{+pH-pK_{a,2}} + 1}{P_{\pm/0}} \tag{3}$$

The logarithmic form of eq 3 describes a somewhat flattened parabolic curve (see Figure 4, dashed curves), characterized by a horizontal region (indicating apparent intrinsic zwitterionic/ampholyte permeability) and two diagonal regions (slope of ±1), below $pK_{a,1}$ and above $pK_{a,2}$. In the bend of the membrane curve (slope one-half), the pH is indicative of the pK_a of the molecule.

Absorption Prediction with "in Combo" PAMPA. The effective permeability coefficients were last modified to include the in silico paracellular correction term based on the Caco-2 model (above). For the intestinal cell membrane barrier, the effective passive permeability, P_e^{INT}, may be defined as

$$\frac{1}{P_e^{INT}} = \frac{1}{P_{ABL}} + \frac{1}{P_{mem} + P_{para}} \tag{4}$$

Equation 4 consists of both measured (P_{mem}) and calculated (P_{ABL} and P_{para}) components; similar combination PAMPA methods have been called "in combo".[21] Equation 4 has the in silico term corresponding to the paracellular permeability, P_{para}, expected in intestinal transport (but not measured in PAMPA). The latter coefficient describes the diffusion of molecules through the aqueous pores in the adjoining junctions between the intestinal epithelial cells. The value of P_{para} was estimated according to eq 1, with *p*CEL-X incorporating the refined (ε/δ), R, and $\Delta\varphi$ parameters best describing the paracellular properties. h_{ABL} is assumed here to be 0.05 cm.[23] At the average fasted-state jejunal pH 6.5, eq 4 may be related to the PAMPA-determined zwitterion/ampholyte intrinsic permeability, $P_{\pm/0}$, as

$$\frac{1}{P_e^{INT}} = \frac{0.05}{10^{-4.131-0.453\log MW}} + \frac{1}{P_{para} + P_{\pm/0}/(10^{-6.5+pK_{a,1}} + 10^{+6.5-pK_{a,2}} + 1)} \tag{5}$$

The P_e^{INT} values calculated by eq 5 were chosen to model human intestinal absorption.

Absorption Curve as a Function of P_e^{INT}. The human absorption data (%F) were fitted against the plug-flow absorption model[24]

$$\%F = A(1 - \exp(-B \cdot P_e^{INT})) \tag{6}$$

where A and B are fitting constants.

Results and Discussion

Paracellular Analysis. Table 1 lists the data[18] used for the new paracellular analysis and summarizes the results of the nonlinear regression. The refined parameters were: $(\varepsilon/\delta) = 0.78 \pm 0.36\ \text{cm}^{-1}$, $R = 12.9 \pm 1.6$ Å, and $\Delta\varphi = -30 \pm 3$ mV. Our paracellular model is different from that described by Adson and co-workers[18,20] in several ways: (a) by the choice of paracellular marker compounds, it had been implicitly assumed by Adson and co-workers that P_{ABL} and P_{trans} contributions to P_{app} could be neglected; (b) the (ε/δ) ratio was calculated after an averaged value of R was determined from a series of pairwise ratios of P_{app}; (c) standard deviations in the measured P_{app} were not taken into account in their calculations; (d) D_{aq} values were calculated from the Stokes−Einstein equation (we used an empirical equation based on measured D_{aq} values for drug-like molecules); and (e) molecular radii were calculated from the molar volume (we used the Sutherland−Stokes−Einstein equation[22]). In our reanalysis, no assumptions were made about the marker molecules being 100% paracellular (P_{app} was calculated as eq 4 and P_{trans} was described as a function of log D_{oct} (see Table 1)), the paracellular parameters were determined simultaneously, and the published individual standard deviations in the P_{app} measurements were utilized for the weighting in the regression analysis. Our approach,

Table 1. Data for Paracellular Analysis of Human Jejunal Permeability[a]

compd	log P_{app}^{Caco-2}	log P_{app}^{calc}	log P_{para}	log P_{trans}	%Para	log D_{OCT}	MW	D_{aq} (10^{-6} cm^2 s^{-1})	r(Å)	$f_{(\pm/0)}$	$f_{(+)}$	$f_{(-)}$	$E(\Delta\varphi)$
methylamine	−5.16 ± 0.03	−5.12	−5.1	−8.5	96	−3.68	31	15.6	2.6	0.0	1.0	0.0	1.65
urea	−5.37 ± 0.04	−5.49	−5.5	−7.3	96	−1.66	60	11.6	2.7	1.0	0.0	0.0	1.00
acetate	−5.78 ± 0.02	−5.77	−5.8	−8.1	98	−3.18	60	11.6	2.7	0.0	0.0	1.0	0.55
hippurate	−6.17 ± 0.02	−6.16	−6.2	−8.3	98	−3.44	179	7.0	3.6	0.0	0.0	1.0	0.55
mannitol	−5.93 ± 0.07	−5.90	−5.9	−8.1	98	−3.10	182	7.0	3.6	1.0	0.0	0.0	1.00
D-Phe-Gly	−5.98 ± 0.12	−6.08	−6.1	−7.6	96	−2.16	222	6.4	3.9	0.6	0.0	0.4	0.80
atenolol	−5.82 ± 0.17	−5.86	−5.9	−7.4	95	−1.92	266	5.9	4.2	0.0	1.0	0.0	1.64
atenolol[b]	−5.89 ± 0.17	−5.86	−5.9	−7.9	97	−2.82[b]	266	5.9	4.2	0.0	1.0	0.0	1.65
D-Phe_2-Gly	−6.26 ± 0.09	−6.34	−6.4	−7.2	85	−1.46	369	5.1	4.7	0.5	0.0	0.5	0.77
D-Phe_3-Gly	−6.44 ± 0.09	−6.40	−6.6	−6.8	56	−0.66	517	4.4	5.4	0.5	0.0	0.5	0.77

[a] All permeability coefficients are in units of cm s^{-1}. The 25 °C Caco-2 P_{app} at pH 7.4 (except as noted below) were taken from Adson et al.[18] %Para is the relative fraction of transport effected by the paracellular route; the %Trans (transcellular) ranged from 0 to 29% and %ABL ranged from 1 to 3% (log P_{ABL} = −3.7 to −4.2). Log D_{OCT} is the octanol−water distribution coefficient at pH 7.4. The molecular radius, r, was calculated by Sutherland−Stokes−Einstein spherical-molecule equation (see text). The $f_{(\pm/0)}$, $f_{(+)}$, and $f_{(-)}$ are the concentration fraction in the uncharged (zwitterion/neutral), cationic, and anionic forms, respectively. $E(\Delta\varphi)$ is the factor due to the potential drop across the cell junction (see text). [b] P_{app}^{Caco-2} and D_{OCT} at pH 6.5.

therefore, is computationally more rigorous and thus may be more generalized. One somewhat surprising outcome of the generalized analysis was that the (ε/δ) and R parameters are highly collinear, with a large negative correlation coefficient above 90%. Nonetheless, the high quality of the published Caco-2 data[18] for the nine paracellular marker molecules allowed for determination of the individual parameters.

Figure 3 shows a plot of log P_{app}^{Caco-2} − log D_{aq} vs the molecular radius of the marker molecules. (By separating the aqueous diffusivity from the apparent permeability, the curves are normalized for molecules size.) The solid line corresponds to the uncharged-species function (eq 1 with $E(\Delta\varphi) = 1$), whereas the dashed lines correspond to the electric-gradient affected function for cations (upper most, $E(\Delta\varphi) > 1$) and the anions (lower most, $E(\Delta\varphi) < 1$). The potential gradient of −30 mV was used to calculate the dashed curves.

Seven of the marker molecules permeated Caco-2 monolayers by the paracellular route predominantly at 95−99%. The two largest molecules, a tri- and a tetrapeptide with molecular weights 369 and 517 Da (Table 1), also permeated mainly by the paracellular route (85% and 56%, respectively). This may be a surprising outcome given the high molecular weights of the two molecules. Although it is true that molecules with molecular weight > 200 Da are not likely to be well-absorbed as a consequence of permeation solely via the paracellular route, conversely it is apparently *not* true that molecules with molecular weights greater than 500 Da cannot permeate via the paracellular route, with triphenylalanylglycine being a case in point (Table 1). This molecule has the predicted $P_{para} = 0.29 \times 10^{-6}$ and $P_{trans} = 0.11 \times 10^{-6}$ cm s^{-1}. If the Caco-2 model[19] accurately depicts the role of paracellular permeation in the human intestine, then all the amphoteric drugs investigated here are expected to permeate to some extent, however small, via the paracellular route. For lipophilic ampholytes, however, the transcellular route predominates over the paracellular route, especially because the luminal membrane surface accounts for more than 99.99% of the total surface in epithelial cells, given the low porosity associated with the paracellular junctions.[20] It appears that there is no obvious practical molecular weight cutoff for the paracellular route.

PAMPA Measurements and the in Combo Descriptor. Table 2 lists the in combo P_e^{INT} values deduced at the gradient pH 6.5. The effective permeability values ranges

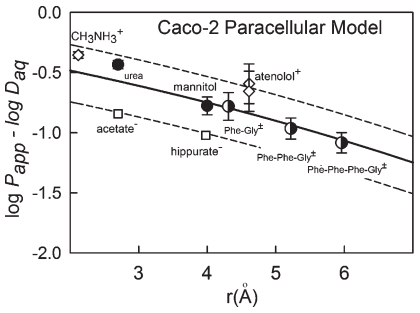

Figure 3. Plot of the Caco-2 data[18] log P_{app} − log D_{aq} vs molecular radius for paracellular markers. The solid line corresponds to the neutral compounds (urea, mannitol, and partly the three peptides); the raised dashed line corresponds to the positively charged molecules (methylamine and atenolol), and the lowered dashed line corresponds to the best fit of negatively charged molecules (acetate and hippurate). The fitting method is described in the Theoretical Section.

from 0.2 × 10^{-6} (ceftazidime, **4**) to 84 × 10^{-6} cm s^{-1} (melphalan, **21**), with a mean value of 14 × 10^{-6} cm s^{-1}. This is a typical range of permeability values reported in many Caco-2 studies of orally administered drugs.[20]

Figure 4 shows the permeability-pH profiles for six selected ampholytes. As mentioned in the Theoretical Section, flattened parabolic curves are expected for the permeability of ampholytes as a function of pH. These membrane permeability profiles are represented by the dashed curves. The solid curves (calculated by eq 5) represent the effective (observable) permeability. In some instances, these curves are depressed from the expected dashed-curve profiles when the aqueous boundary layer (dotted line) limits permeation, as in the case of parts a, b, d of Figure 4 (meloxicam, cerivastatin, and benazepril). The effective (solid line) curves decrease past the limits of the two pK_a values, and again level off at a low permeation value, due to the shunting effect of the expected paracellular permeability, as, e.g., for fexofenadine for pH < 3, daunorubicin for pH < 6, and sulfadiazine for pH > 7. The underlying paracellular contributions are indicated by dash−dot curves in Figure 4. These were calculated according to the method described in the Theoretical Section. The circle points on the solid curves are values of P_e^{INT}, which were selected to model human absorption.

Because of the pH microclimate adjacent to the surface of the epithelium (pH 6.5 near the tips of the villi[48]), the

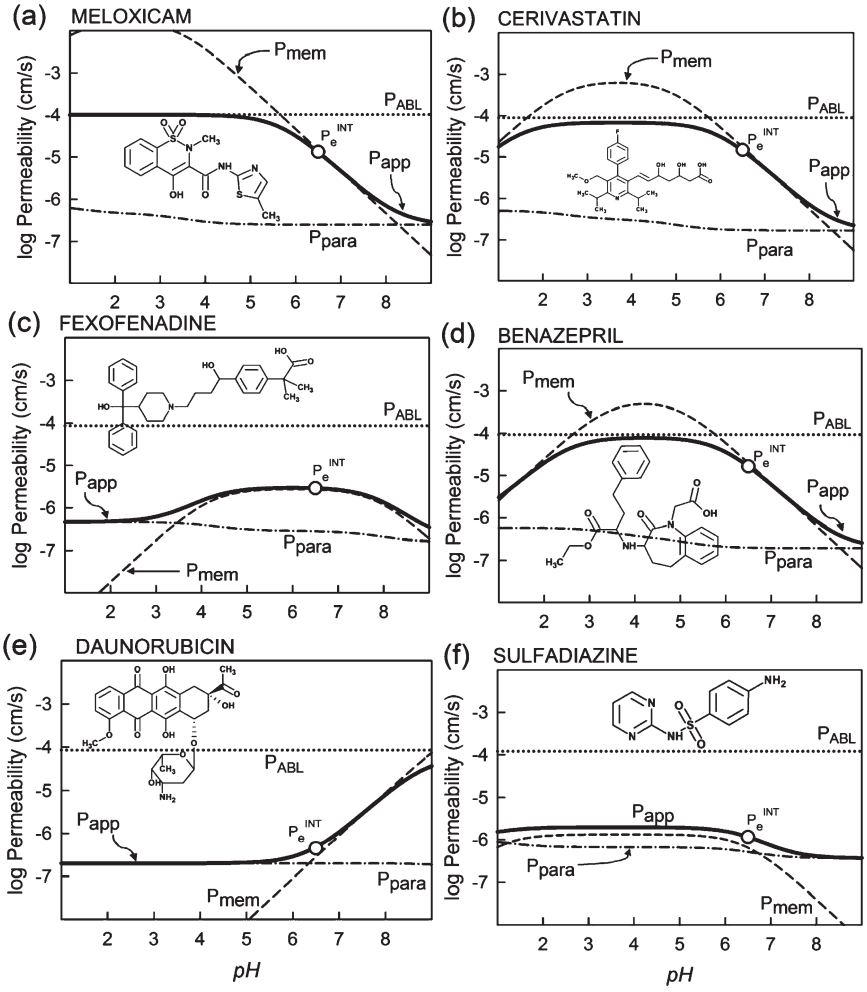

Figure 4. Log permeability vs pH profiles of six of the ampholytes. Solid curves correspond to the effective (observable) permeability (calculated by eq 5). The dashed curves are due to the membrane permeability, P_{mem} (cf., eq 3), and have the expected parabolic shapes. The paracellular permeability, P_{para}, is shown as dash−dot curves (calculated by eq 1). The dotted curves represent the aqueous boundary layer permeability, P_{ABL} (see text). The solid curves are confined to the 2−3 orders of magnitude permeability window formed by the shunting effect of P_{para} and the limiting resistive effect of P_{ABL}.

expected permeation of meloxicam, cerivastatin, and benazepril (and other moderately lipophilic ampholytes with the higher pK_a value <6) may be quite sensitive to local pH changes, particularly in the pH region 6−8 (Figure 4). As reported by Daniel et al.,[48] the microclimate pH can be as high as 8.0−8.5 in the intervillus space, about 200−400 μm below the villus tips in the small intestine. Table 2 also lists the pK_a and the human absolute bioavailability (%F) values used in the study. Of the 33 drugs studied, a third of the drugs are predicted to permeate the intestinal barrier by the paracellular route predominantly, with acyclovir, ceftazidime, daunorubicin, famotidine, ganciclovir, levocarnithine, and terbutaline being nearly entirely transported via the paracellular route but with a low average absorption of $<14\%$ (Table 2). This high paracellular fraction is somewhat surprising, given the discussions surrounding the human jejunal permeability measurements by Lennernäs and co-workers, who had suggested that paracellular route may not be as important as that of the passive transcellular route in intestinal absorption for the 42 compounds (mostly drugs) tested in humans so far.[49] However, this could be that most of the compounds whose jejunal permeability has been determined are not ampholytes such as those considered here, although some molecules are included in both studies.

Also shown in Table 2 are the predominant charges of the compounds at pH 6.5. About 64% of the compounds are mainly in the zwitterionic form and about 18% are mainly anionic. The remaining compounds are predominantly neutral (acyclovir, ganciclovir, and torsemide) or cationic (daunorubicin, famotidine, and terbutaline).

Almost all of the ampholytes whose bioavailability is $<50\%$ permeate via the paracellular route predominantly ("checkered" symbols in Figure 5), with fexofenadine and benazepril being exceptions. Of this paracellular set of ampholytes, nearly half are zwitterions (Table 2). Benazepril is not part of the "checkered" paracellular set, quite likely because it is an outlier in the study (see below). Fexofenadine is not characteristic of the "checkered" paracellular set due to its elevated PAMPA permeability. On the basis of the PAMPA data, the molecule would have been expected to have somewhat higher human bioavailability. Fexofenadine is known to be a substrate of P-gp and OAT.[50,51] The drug has been on the market for over a decade. However, it has not been reported as administrated intravenously in human until 2008. The absolute bioavailability data available in open literature were an estimate based on recovery data.[40] The drug is only slightly metabolized. The modest bioavailability of fexofenadine has been attributed partly to low intestinal

Table 2. Experimental in Combo Permeability, pK_a, and the Absolute Bioavailability of the Compounds

compd	P_e^{INT} (pH 6.5) (10^{-6} cm/s)	%Para	pK_a	charge state at pH 6.5	human absolute bioavailability (%F)
acyclovir (**1**)	0.8	99	2.34, 9.23[8]	0	21[39] (15− 50)[43]
amdinocillin (**2**)	0.9	46	2.2, 9.1[25]	±	10[39]
benazepril (**3**)	17	1	3.4, 5.0[25]	−	37[40]
ceftazidime (**4**)	0.2	96	2.55[8]	±	0[39] (< 10)[43]
cerivastatin (**5**)	15	1	2.48, 4.90 [a]	−	60 (39− 101)[40]
cetirizine (**6**)	42	0	2.93, 8.00[26]	±	> 80[41]
chlortetracycline (**7**)	3.7	5	3.30, 7.44[27]	±,−	60[39] (25−60)[42]
ciprofloxacin (**8**)	2.8	18	6.16, 8.62[28]	±,+	70[40]
daunorubicin (**9**)	0.3	99	9.7, > 11[d]	+	0[39]
demeclocycline (**10**)	3.8	4	3.97, 6.76 [a]	±,−	66[42]
doxycycline (**11**)	20	1	3.13, 7.69 [b,8]	±	93[43]
enoxacin (**12**)	7.7	6	6.30, 8.70[29]	±,+	89[44]
famotidine (**13**)	0.6	98	6.74, 11.19[8]	+,0	42 (40−45)[45]
fexofenadine (**14**)	2.8	6	4.20, 7.84 [b,30]	±	30[41] (30− 40)[52]
ganciclovir (**15**)	0.7	99	2.34, 9.23 [c]	0	7.3[39]
gatifloxacin (**16**)	20	1	5.90, 9.30[31]	±,+	96[40]
levocarnitine (**17**)	1.3	98	3.8[32]	±	10[39]
lisinopril (**18**)	0.6	45	3.16,7.32 [a]	±,−	25[39]
lomefloxacin (**19**)	15	2	5.50, 8.80[33]	±	97[39] (95−98)[40]
meloxicam (**20**)	13	1	1.1, 3.43[8,34]	−	89[40]
melphalan (**21**)	84	0	2.0, 9.4[25]	±	71 (±23)[43]
mesalamine (**22**)	0.9	90	2.70, 5.80[35]	−,0	28[40]
minocycline (**23**)	50	0	5.07, 7.61 [b]	±	100[43]
norfloxacin (**24**)	1.0	56	6.26, 8.63[28]	±,+	35 (30−40)[40]
ofloxacin (**25**)	4.7	8	6.05,8.35[28]	±,+	90[39]
pefloxacin (**26**)	23	1	6.27,7.81[28]	±,+	95[46] (80−110)[43]
piroxicam (**27**)	20	1	1.88, 5.07[8,36]	−	100[43]
sparfloxacin (**28**)	42	0	5.92, 8.66[28]	±,+	92[40]
sulfadiazine (**29**)	1.2	45	1.0, 6.48[25]	−,0	100[39]
terbutaline (**30**)	1.4	99	8.67, 10.12[8,37]	+	14[39] (22 ± 9)[43]
tetracycline (**31**)	3.8	6	3.01, 7.85 [b]	±	78[43] (77−80)[42]
torsemide (**32**)	22	1	2.6, 6.70[38]	0,−	80[45] (91)[43]
trovafloxacin (**33**)	57	0	5.90, 8.11[8]	±,+	88 (65−122)[47]

[a] This work. [b] Refined from log P_e vs pH data, using the *p*CEL-X v2.0 program. [c] Assumed to be the same as that of acyclovir. [d] Estimated based on pK_a values of doxorubicin.[8]

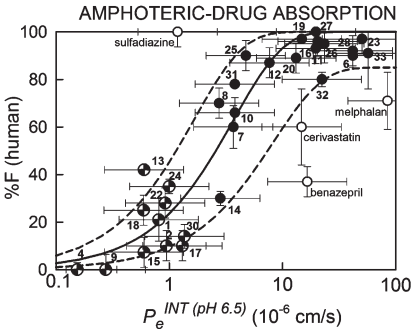

Figure 5. Human absolute oral bioavailability plotted against the P_e^{INT} in combo PAMPA gradient pH 6.5 permeability values for the 33 ampholytes studied. The solid curve is the best fit of the function represented by eq 6. The dashed curves are based on estimated errors in the log P_e^{INT} values (±0.35). The points in solid circles represent molecules where the dominant mode of transport is by passive transcellular diffusion. The checkered-circles represent molecules that permeate (poorly) by the paracellular route primarily. The unfilled circles represent outliers: three false positives and two false negatives.

permeability, as the Caco-2 cell permeability of the molecule is low (even in the presence of potent P-gp inhibitors).[41] Recently, the intravenous pharmacokinetics and absolute bioavailability of fexofenadine was determined.[52,53] The absolute bioavailability is reported to be between 30−40%. It has been suggested that the molecule could be eliminated predominately by biliary excretion, and P-gp and OAT could have a key role in this process.[52,53] For molecules, such as fexofenadine, exhibiting a mixture of excretion and transporter issues, passive permeability on its own may not be sufficient to fully rationalize the exposure/oral bioavailability data. We recommend taking into consideration the metabolic and transporter data to gain a better understanding on the absorption process.

Prediction of Human Absorption. Figure 5 shows the absolute bioavailability of the 33 ampholytes as a function of the P_e^{INT} values deduced at the gradient pH 6.5, with the solid curve represents the best fit to eq 6. The best-fitted parameters are: $A = 100$, $B = 0.27 \times 10^{+6}$. The dashed curves are based on estimated errors in the log P_e^{INT} values (±0.35). For the upper dashed curve, parameter A is 100, while a value of 85 is used for the lower dashed curve (in part, to reflect the estimated errors in the %F data). For most of the ampholytes studied in this work, the estimated errors in the %F data could be up to ±16% (excluding melaphalan, see below). This is based on the assumption of a 95% confident interval from different published %F values where available. (In instances where errors in the published %F values are not available, the average value, 6%, based on known errors from the rest of the molecules was assumed.) The points in solid circles represent molecules where the dominant mode of transport is by passive transcellular diffusion, while the checkered circles represent molecules that permeate (poorly) by the paracellular route primarily as

predicted in our model. On the basis of this model, the P_e^{INT} values for 50% predicted human bioavailability could be estimated to be 2.6×10^{-6} cm s^{-1}.

The absolute bioavailability data presented in Table 2 and Figure 5 have not been corrected for first pass metabolism. We have carefully selected molecules, which have low to moderate in vivo clearance in human[54] (i.e., do not show significant metabolic liability). For most of the molecules studied in this work, the difference between the absolute bioavailability with or without the correction of in vivo clearance (first pass effects) is less than 15%, except: ciprofloxacin, enoxacin, melphalan, and famotidine. Ciprofloxacin and enoxacin already showed high absolute bioavailability, not too far from 100% absorption. While for the other two molecules, we will discuss in a greater detail in the subsequent section. Fexofenadine showed a relatively high in vivo clearance, which is believed to be mainly due to biliary excretion[52,53] (see above). The correction for first pass effects for this molecule is not relevant. It can be seen that the human absorption of most of the ampholytes was generally well predicted by the approach used here. There were five outliers, however (3 false positive, 2 false negatives).

False Positives. Melphalan (21). Melphalan is an L-amino acid transporter (LAT1) substrate, but its affinity to LAT1 is not high.[55] This compound exhibits variable bioavailabiliy. Sietsema[43] reported the bioavailability of melphalan as 72% (range 48−94%, SD = 12%) (cited from three different references). The variations could be due to a combination of factors, e.g., dose adjustment needed due to adverse toxicological effects (melphalan is a nitrogen mustard drug for cancer treatment) and poor aqueous solubility of the compound.[40] Moreover, the compound is eliminated by chemical hydrolysis to monohydroxymelphalan and dihyroxymelphalan,[40] with in vivo clearance about 30% of the human liver blood flow.[54] This is relatively high compared with most of the compounds in this study. Correction for the clearance (assuming metabolism is the major route of elimination) gives a %F value very close to 100%, which is consistent with the prediction generated in our model.

Cerivastatin (5). The in vivo clearance of cerivastatin is about 10% human liver blood flow.[54] However, the bioavailability could vary greatly (range 39−101%[40]), which is due to intersubject variability. Again our model is able to predict a value within the experimental error range.

Benazepril (3). Benazepril is an ester prodrug of benazeprilat. Following oral absorption, the prodrug is completely hydrolyzed (primarily in the liver) to benazeprilat.[56] The human absorption data is estimated by urinary recovery.[40] It is plausible that these data are underestimated to some extent because of the fast hydrolysis reaction in vivo. This may lead to an overestimated prediction generated in our model.

False Negative. Famotidine (13). Famotidine has been reported as a substrate of the renal organic anion transporter (hOAT3), which may mainly affect urinary drug excretion.[57] The in vivo clearance is about 16% of the human liver blood flow,[54] which barely exceeds the threshold of 15% we set out for compound selection (see above). Recently, the intestinal permeability of famotidine has been studied.[58] The molecule exhibited segmental dependent transport behavior in human intestine. It has been shown that the permeability is higher in the proximal intestinal region than that of the distal intestinal region, which is consistent with the P-gp expression level being lower in the proximal region (but higher in the distal region).[58] From these literature evidence, hOAT3 and/or P-gp and might have some impact on the bioavailability of famotidine. The PAMPA permeability of famotidine is very low in our case (experimentally challenging to determine), and the transport is predicted to be entirely paracellular driven in the absorption model. It is plausible that the "Adson model" adopted in our paracellular analysis may not be a perfect model for mimicking the human intestine, leading to some extra degree of uncertainty in the prediction. Nevertheless, the prediction is not too distant from the bioavailability data.

Sulfadiazine (29). Sulfadiazine has a low octanol−water partition coefficient (log $P_{OCT} = -0.08$) and shows only moderate permeability in the PAMPA assay ($P_e^{INT} = 1.2 \times 10^{-6}$ cm s^{-1}). Furthermore, the drug is about 51% negatively charged at pH 6.5. These physicochemical characteristics usually are not predictive of compounds that are 100% absorbed. We are not aware of any studies describing sulfadiazine as a substrate of anionic transporters.

Sensitivity of our Absorption Model. As shown in Figure 5, our absorption model is able to predict 28 out of 33 molecules correctly (~85%) within the experimental uncertainty of the in combo P_e^{INT} values. This set of 33 compounds covers several distinct chemical series. Generally, in a drug-hunting project, the focus would be to drive one (or more) lead series against a particular biological target. Good oral exposure is usually required to ensure sufficient drug concentration to hit the biological target of interest and to elicit the desirable pharmacological response. It would be of great interest to interrogate whether our absorption model could rank the molecules within the same chemical series in the right order in terms of absorption.

The first example is the antihistamine: cetirizine (**6**) and fexofenadine (**14**). As shown in Table 2, the P_e^{INT} of cetirizine is 14-fold higher than that of fexofenadine, which is in consistent with the higher bioavailability of cetirizine than that of fexofenadine. Next, attention is directed to antibacterials. The data of β-lactams (amdinocillin (**2**) vs ceftazidime (**4**)) illustrated that the model is able to differentiate the small difference in bioavailability. Moreover the model is able to spot norfloxacin (**24**) as the poorly absorbed entity from the others within the fluoroquinolone series (e.g., molecules **8**, **12**, **16**, **19**, **25**, **26**, **28**, and **33**). Likewise, the model performs well on the tetracycline series, as it is able to differentiate the relatively poorly absorbed chlortetracycline (**7**), demeclocycline (**10**), and tetracycline (**31**) out of the well absorbed members: doxycycline (**11**) and minocycline (**23**). Most interestingly, the very poorly absorbed anthracycline glycoside analogue, daunorubicin (**9**), can be clearly identified by the P_e^{INT} values. It can be seen that the sensitivity of our absorption model is satisfactory. We have demonstrated that the in combo P_e^{INT} data could be used to identify poorly absorbed entities within a chemical series.

Conclusion

We have studied 33 amphoteric drugs in the parallel artificial membrane permeability assay (PAMPA). A generalized paracellular permeability model based on Caco-2 cell permeability data has been developed to enhance the PAMPA permeability data. It was found that these "in combo" PAMPA data correlate well with the human absolute bioavailability of the ampholytes via a plug-flow absorption model. Among these 33 amphoteric drugs, five outliers have been identified, which could be rationalized by transporters and/or

metabolic issues, as well as the possible microclimate pH effects in the intestine. Our data suggests that majority of these ampholytes exhibit certain degrees of paracellular transport, which is becoming the major route of transport for ampholytes of low bioavailability (e.g., < 50%). We have demonstrated that the absorption model developed in this work is very sensitive in the identification of poorly absorbed (or well absorbed) molecules, even within structurally related chemical series. It is envisaged that the model would be useful in drug hunting project to help the prioritization of the most promising candidates for pharmacokinetics studies.

Experimental Section

Chemicals Used. Acyclovir, lisinopril, terbutaline, and famotidine were purchased from Sigma-Aldrich (St. Louis, MO). Ofloxacin and pefloxacin were kind gifts from Prof. Marival Bermejo (Valencia University, Spain). Other compounds were supplied by AstraZeneca (Macclesfield, UK). The Double-Sink PAMPA lipid was obtained from *p*ION (PN 110669) and was stored at −20 °C when not used. The pH of the assayed donor solutions was adjusted with the Prisma universal buffer (*p*ION, PN 100621). The pH 7.4 surfactant-containing buffer (*p*ION, PN 110158) was used as the receiver solution.

pK_a Measurement. The potentiometric Gemini Profiler (*p*ION INC, Woburn, MA) instrument was used to determine precision ionization constants of cerivastatin, demeclocycline, and lisinopril at 25 ± 0.5 °C and 0.15 M ionic strength (KCl). Details of the procedure have been described elsewhere.[8] Electrode calibration was performed "in situ", concurrently with the pK_a determination. This is a substantial improvement in comparison to the traditional procedure of first doing a "blank" titration to determine the four Avdeef−Bucher pH electrode parameters.[14]

The Parallel Artificial Membrane Permeability Assay (PAMPA). The PAMPA Evolution instrument (*p*ION) was used, with permeability data collected at room temperature (25 ± 2 °C). The 96-well PAMPA "sandwich" was preloaded with 96 magnetic stirrers (*p*ION, PN 110212). The typical sample concentrations were about 50 μM. The effective permeability, P_e, of each compound was measured at the isoelectric pH (pH_{IEP}). The donor buffers were automatically prepared by the robotic instrument with the additions of predetermined amounts of standardized NaOH to the universal pH buffer. The pH 7.4 receiver buffer solutions contained a surfactant mixture ("lipophilic sink") to mimic some of the function of drug-binding proteins.[8] For the highly permeable molecules (e.g., benazepril, cerivastatin, meloxicam, piroxicam, sparfloxacin, torsemide, and trovafloxacin), the PAMPA sandwich was allowed to incubate for 30 min under vigorous stirring in a controlled-environment chamber (Gut-Box, *p*ION, PN 110205) with a built-in magnetic stirring mechanism with the dial set at 40 μm (aqueous boundary layer thickness). The remaining (more hydrophilic) zwitterions were allowed to incubate for 15 h in a saturated humidity environment, without stirring. The sandwich was then separated, and both the donor and receiver wells were assayed for the amount of material present by comparison with the UV spectrum (230−500 nm) obtained from reference standard solutions. Mass balance was used to determine the amount of material remaining in the membrane filter (%R) and attached to the plastic walls of the microtiter plate.[8]

The effective permeability (P_e) was calculated as described previously,[8] except that the usable filter area, 0.3 cm^2, was multiplied by the apparent porosity, 0.76. This latter step ensures that the ABL thickness determined from PAMPA assays using filters with a different porosity would be on an absolute scale.[10]

Acknowledgment. We wish to thank Prof. Marival Bermejo of the University of Valencia, Spain, for useful discussion concerning the absorption properties of fluoroquinolones, and the gift of two of the compounds used in this study. Thanks are due to Prof. Malcolm Rowland (the University of Manchester, UK) and Dr. Andy Thomas (AstraZeneca, UK) for helpful discussions. *p*ION's research was self-funded, as was that of AstraZeneca.

References

(1) Pagliara, A.; Carrupt, P. A.; Caron, G.; Gaillard, P.; Testa, B. Lipophilicity profiles of ampholytes. *Chem. Rev.* **1997**, *97*, 3385–3400.
(2) WHO Expert Committee. *The Use of Essential Drugs*; WHO: Geneva, 1995.
(3) Ings, R. M. J. Pharmacokinetics. In *Medicinal Chemistry: Principles and Practice*; King, F. D., Ed.; RSC: Cambridge, 1994 pp 67−85.
(4) Jamieson, C.; Moir, E. M.; Rankovic, Z.; Wishart, G. Medicinal chemistry of hERG optimizations: highlights and hang-ups. *J. Med. Chem.* **2006**, *49*, 5029–5046.
(5) Breedveld, P.; Beijnen, J. H.; Schellens, H. M. Use of P-glycoprotein and BCRP inhibitors to improve oral bioavailability and CNS penetration of anticancer drugs. *Trends Pharmacol. Sci.* **2006**, *27*, 17–24.
(6) Petzinger, E.; Geyer, J. Drug transporters in pharmacokinetics. *Naunyn-Schmeideberg's Arch. Pharmacol.* **2006**, *372*, 465–475.
(7) Kansy, M.; Senner, F.; Gubernator, K. Physicochemical high throughput screening: parallel artificial membrane permeability assay in the description of passive absorption processes. *J. Med. Chem.* **1998**, *41*, 1007–1010.
(8) Avdeef, A. *Absorption and Drug Development*; Wiley-Intercience: New York, 2003.
(9) Wohnsland, F.; Faller, B. High-throughput permeability pH profile and high-throughput alkane/water log P with artificial membranes. *J. Med. Chem.* **2001**, *44*, 923–930.
(10) Nielsen, P.; Avdeef, A. PAMPA−A Drug Absorption in vitro Model. 8. Apparent Filter Porosity and the Unstirred Water Layer. *Eur. J. Pharm. Sci.* **2004**, *22*, 33–41.
(11) Avdeef, A.; Tsinman, O. PAMPA—a drug absorption *in vitro* model. 13. Chemical selectivity due to membrane hydrogen bonding: in combo comparisons of HDM-, DOPC-, and DS-PAMPA. *Eur. J. Pharm. Sci.* **2006**, *28*, 43–50.
(12) Avdeef, A.; Bendels, S.; Di, L.; Faller, B.; Kansy, M.; Sugano, K.; Yamauchi, Y. PAMPA—a useful tool in drug discovery. *J. Pharm. Sci.* **2007**, *96*, 2893–2909.
(13) Avdeef, A.; Kansy, M.; Bendels, S.; Tsinman, K. Absorption-excipient-pH classification gradient maps: sparingly-soluble drugs and the pH partition hypothesis. *Eur. J. Pharm. Sci.* **2008**, *33*, 29–41.
(14) Avdeef, A.; Bucher, J. J. Accurate measurements of the concentration of hydrogen ions with a glass electrode: calibrations using the Prideaux and other universal buffer solutions and a computer-controlled automatic titrator. *Anal. Chem.* **1978**, *50*, 2137–2142.
(15) Sugano, K.; Takata, N.; Machida, M.; Saitoh, K.; Terada, K. Prediction of passive intestinal absorption using biomimetic artificial membrane permeation assay and the paracellular pathway model. *Int. J. Pharm.* **2002**, *241*, 241–251.
(16) Saitoh, R.; Sugano, K.; Takata, N.; Tachibana, T.; Higashida, A.; Nabuchi, Y.; Aso, Y. Correction of permeability with pore radius of tight junctions in Caco-2 monolayers improves the prediction of dose fraction of hydrophilic drugs absorbed by humans. *Pharm. Res.* **2004**, *21*, 749–755.
(17) Sugano, K. Theoretical investigation of passive intestinal membrane permeability using Monte Carlo method to generate drug-like molecule population. *Int. J. Pharm.* **2009**, *373*, 55–61.
(18) Adson, A.; Raub, T. J.; Burton, P. S.; Barsuhn, C. L.; Hilgers, A. R.; Audus, K. L.; Ho, N. F. H. Quantitative approaches to delineate paracellular diffusion in cultured epithelial cell monolayers. *J. Pharm. Sci.* **1994**, *83*, 1529–1536.
(19) Reynolds, D. P.; Lanevskij, K.; Japertas, P.; Didziapetris, R.; Petrauskas, A. Ionization-specific analysis of human intestinal absorption. *J. Pharm. Sci.* **2009**, *98*, 4039–4054.
(20) Ho, N. F. H.; Raub, T. J.; Burton, P. S.; Barsuhn, C. L.; Adson, A.; Audus, K. L.; Borchardt, R. Quantitative approaches to delineate passive transport mechanisms in cell culture monolayers. In *Transport Processes in Pharmaceutical Systems*; Amidon, G. L., Lee, P. I., Topp, E. M., Eds.; Marcel Dekker: New York, 2000; pp 219−316.
(21) Avdeef, A.; Artursson, P.; Neuhoff, S.; Lazarova, L.; Grasjö, J.; Tavelin, S. Caco-2 permeability of weakly basic drugs predicted

with the Double-Sink PAMPA pK_a^{flux} method. *Eur. J. Pharm. Sci.* **2006**, *24*, 333–349.
(22) Avdeef, A. Leakiness and Size Exclusion of Paracellular Channels in Cultured Epithelial Cell Monolayers—Interlaboratory Comparison. Unpublished results.
(23) Winne, D. Dependence of intestinal absorption in vivo on the unstirred layer. *Nauyn-Schmiedeberg's Arch. Pharmacol.* **1978**, *304*, 175–181.
(24) Yu, L. X.; Amidon, G. L. A compartmental absorption and transit model for estimating oral drug absorption. *Int. J. Pharm.* **1999**, *186*, 119–125.
(25) Predicted values using Pharma Algorithms ADME Boxes Rev. 4.9.
(26) Pagliara, A.; Testa, B.; Carrupt, P. A.; Jolliet, P.; Morin, C.; Morin, D.; Urien, S.; Tillement, J. P.; Rihoux, J. P. Molecular properties and pharmacokinetic behavior of cetirizine, a zwitterionic H_1-receptor antagonist. *J. Med. Chem.* **1998**, *41*, 853–863.
(27) Leeson, L. J.; Krueger, J. E.; Nash, R. A. Concering the structural assigment of the second and third acidity constants of the tetracycline antibiotics. *Tetrahedron Lett.* **1963**, *18*, 1155–1160.
(28) Bermejo, M.; Avdeef, A.; Ruiz, A.; Nalda, R.; Ruell, J. A.; Tsinman, O.; González, I.; Fernández, C.; Sánchez, G.; Garrigues, T. M.; Merino, V. PAMPA—a drug absorption in vitro model. 7. Comparing rat in situ, Caco-2, and PAMPA permeability of fluoroquinolones. *Eur. J. Pharm. Sci.* **2004**, *21*, 429–441.
(29) Ross, D. L.; Riley, C. M. Physicochemical properties of the fluoroquinolone antimicrobials. II. Acid ionization constants and their relationship to structure. *Int. J. Pharm.* **1982**, *83*, 267–272.
(30) Omari, M. M. A.; Zughui, M. B.; Davies, J. E. D.; Badwan, A. A. Thermodynamic enthalpy−entropy compensation effects observed in the complexation of basic drug substrates with β-cyclodextrin. *J. Inclusion Phenom. Macrocyclic Chem.* **2007**, *57*, 379–384.
(31) Ooie, T.; Suzuki, H.; Terasaki, T.; Sugiyama, Y. Comparative Distribution of Quinolone Antibiotics in Cerebrospinal Fluid and Brain in Rats and Dogs. *J. Pharmacol. Exp. Ther.* **1996**, *278*, 590–596.
(32) Yalkowsky, S. H.; Zografi, G. Potentiometric Titration of Monomeric and Micellar Acylcarnitines. *J. Pharm. Sci.* **1970**, *59*, 798–802.
(33) Takács-Novák, K.; Noszál, B.; Hermecz, I.; Keresztúri, G.; Podányi, B.; Szász, G. Protonation Equilibria of Quinolone Antibacterials. *J. Pharm. Sci.* **1990**, *79*, 1023–1028.
(34) Abdoh, A. A.; El-Barghouthi, M. I.; Zughui, M. B.; Davies, J. E.; Badwan, A. A. Changes in the conformational structure, microscopic and macroscopic pK_as of meloxicam on complexation with natural and modified cyclodextrins. *Pharmazie* **2007**, *62*, 55–59.
(35) Fallab, S; Vögtli, W; Blumer, M Erlenmeyer. Zur Kenntnis. der *p*-aminosalicylsäure. *Helv. Chim. Acta* **1951**, *34*, 26–27.
(36) Takács-Novák, K.; Tam, K. Y. Multiwavelength spectrophotometric determination of acid dissociation constants. Part V: Microconstants and tautomeric ratios of diprotic amphoteric drugs. *J. Pharm. Biomed. Anal.* **2000**, *12*, 1171–1182.
(37) Takács-Novák, K.; Noszál, B.; Tokeskovesdi, M.; Szász, G. Acid−base properties of terbutaline in terms of protonation macro- and microconstants. *J. Pharm. Pharmacol.* **1995**, *47*, 431–435.
(38) Wouters, J.; Michaux, C.; Durant, F.; Dogné, J. M.; Delarge, J.; Masereel, B. Isoterism among analogues of torsemide: conformational, electronic and lipophilic properties. *Eur. J. Med. Chem.* **2000**, *35*, 923–930.
(39) Dollery, C. T. *Therapeutic Drugs*, 2nd ed.; Churchill Livingstone: New York, 1999.
(40) FDA Drug Information (http://www.fda.gov/Drugs/default.htm).
(41) Whomsley, R.; Benedetti, M. S. Development of new H1 antihistamines: the importance of pharmacokinetics in the evaluation of safe and therapeutically effective agents. *Curr. Med. Chem.—Anti-Inflammatory Anti-Allergy Agents* **2005**, *4*, 451–464.
(42) Agwuh, K. N.; MacGowan, A. Pharmacokinetics and pharmcodynamics of the tetracyclines including glycylcyclines. *J. Antimicrob. Chemother.* **2006**, *58*, 256–265.
(43) Sietsema, W. K. The Absolute Oral Bioavailability of Selected Drugs. *Int. J. Clin. Pharmcol. Ther. Toxicol.* **1989**, *27*, 179–211.
(44) Hinderling, P. H. Evaluation of a novel method to estimate absolute bioavailability of drugs from oral data. *Biopharm. Drug Dispos.* **2003**, *24*, 1–6.
(45) *Physician's Desk Reference*, 63rd ed.; Thomson Reuters: Montvale, NJ, **2009**.
(46) Frydman, A. M.; Leroux, Y.; Lefebvre, M. A.; Djebbar, F.; Fourtillan, J. B.; Gaillot, J. Pharmacokinetics of Pefloxacin after Repeated Intravenous and Oral-Administration (400 mg bid) in Young Healthy Volunteers. *J. Antimicrob. Chemother.* **1986**, *17* (Suppl. B), 65–79.
(47) Teng, R.; Dogolo, L. C.; Willavize, S. A.; Friedman, H. L.; Vincent, J. Oral bioavailability of trovafloxacin with and without food in healthy volunteers. *J. Antimicrob. Chemother.* **1997**, *39* (Suppl. B), 87–92.
(48) Daniel, H.; Neugerbauer, B.; Kratz, A.; Rehner, G. Localization of acid microclimate along intestinal villi of rat jejunum. *Am. J. Physiol.* **1985**, *248*, G293–G298.
(49) Lennernäs, H. Intestinal permeability and its relevance for absorption and elimination. *Xenobiotica* **2007**, *37*, 1015–1051.
(50) Petri, N.; Tannergren, C.; Rungstad, D.; Lennernäs, H. Transport characteristics of fexofenadine in the caco-2 cell model. *Pharm. Res.* **2004**, *21*, 1398–1404.
(51) Tannergren, C.; Petri, N.; Knutson, L.; Hedeland, M.; Bondesson, U.; Lennernäs, H. Multiple transport mechanisms involved in the intestinal absorption and first-pass extraction of fexofenadine. *Clin. Pharmacol. Ther.* **2003**, *74*, 423–436.
(52) European Microdosing AMS Partnership Programme. Linear pharmacokinetics demonstrated between a microdose and therapeutic dose of the Pgp substrate in humans. In American Society for Clinical Pharmacology and Therapeutics Annual Meeting, Orlando, FL, 2008.
(53) Lappin, G.; Stevens, L. Biomedical accelerator mass spectrometry: recent applications in metabolism and pharmacokinetics. *Expert Opin. Drug Metab. Toxicol.* **2008**, *4*, 1021–1033.
(54) Obach, R. S.; Lombardo, F.; Waters, N. J. Trend analysis of a database of intravenous pharmacokinetic parameters in humans for 670 drug compounds. *Drug Metab. Dispos.* **2008**, *36*, 1385–1405.
(55) del Amo, E. M.; Urtti, A.; Yliperttula, M. Pharmacokinetic role of L-type amino acid transporters LAT1 and LAT2. *Eur. J. Pharm. Sci.* **2008**, *34*, 161–174.
(56) Kaiser, G.; Ackermann, R.; Brechbühler, S.; Dieterle, W. Pharmacokinetics of the angiotensin converting enzyme inhibitor benazepril·HCl (CGS 14 824 A) in healthy volunteers after single and repeated administration. *Biopharm. Drug Dispos.* **1989**, *10*, 365–376.
(57) Motohashi, H.; Uwai, Y.; Hiramoto, K.; Okuda, M.; Inui, K.-I. Different transport properties between famotidine and cimetidine by human renal organic ion transporters (SLC22A). *Eur. J. Pharmacol.* **2004**, *503*, 25–30.
(58) Dahan, A.; Amidon, G. L. Segmental dependent transport of low permeability compounds along the small intestine due to P-glycoprotein: the role of efflux transport in the oral absorption of BCS class III drugs. *Mol. Pharmaceutics* **2009**, *6*, 19–28.
(59) Escher, B. I.; Berger, C.; Bramaz, N.; Kwon, J. H.; Richter, M.; Tsinman, O.; Avdeef, A. Membrane-water partitioning, membrane permeability and nontarget modes of action in aquatic organisms of the parasiticides ivermectin, ablendazole and morantel. *Environ. Toxicol. Chem.* **2008**, *27*, 909–918.